Journal of Virology®

VIRUS-CELL INTERACTIONS

Hepatitis E Virus Protease Inhibits the Activity of Eukaryotic Initiation Factor 2-Alpha Kinase 4 and Promotes Virus Survival

Amit Kumar,[a] Chandru Subramani,[a]* Shivani Raj,[b] C. T. Ranjith-Kumar,[b] Milan Surjit[a]

[a]Virology Laboratory, Translational Health Science and Technology Institute, NCR Biotech Science Cluster, Faridabad, Haryana, India
[b]University School of Biotechnology, Guru Gobind Singh Indraprastha University, New Delhi, India

ABSTRACT Multiple mechanisms exist in a cell to cope with stress. Four independent stress-sensing kinases constitute the integrated stress response machinery of the mammalian cell, and they sense the stress signals and act by phosphorylating the eukaryotic initiation factor 2α (eIF2α) to arrest cellular translation. Eukaryotic initiation factor 2 alpha kinase 4 (eIF2AK4) is one of the four kinases and is activated under conditions of amino acid starvation, UV radiation, or RNA virus infection, resulting in shutdown of global translation. An earlier study in our laboratory constructed the protein interaction network of the hepatitis E virus (HEV) and identified eIF2AK4 as a host interaction partner of the genotype 1 (g1) HEV protease (PCP). Here, we report that PCP's association with the eIF2AK4 results in inhibition of self-association and concomitant loss of kinase activity of eIF2AK4. Site-directed mutagenesis of the 53rd phenylalanine residue of PCP abolishes its interaction with the eIF2AK4. Further, a genetically engineered HEV-expressing F53A mutant PCP shows poor replication efficiency. Collectively, these data identify an additional property of the g1-HEV PCP protein, through which it helps the virus in antagonizing eIF2AK4-mediated phosphorylation of the eIF2α, thus contributing to uninterrupted synthesis of viral proteins in the infected cells.

IMPORTANCE Hepatitis E virus (HEV) is a major cause of acute viral hepatitis in humans. It causes chronic infection in organ transplant patients. Although the disease is self-limiting in normal individuals, it is associated with high mortality (~30%) in pregnant women. In an earlier study, we identified the interaction between the genotype 1 HEV protease (PCP) and cellular eukaryotic initiation factor 2 alpha kinase 4 (eIF2AK4). Since eIF2AK4 is a sensor of the cellular integrated stress response machinery, we evaluated the significance of the interaction between PCP and eIF2AK4. Here, we show that PCP competitively associates with and interferes with self-association of the eIF2AK4, thereby inhibiting its kinase activity. Lack of eIF2AK4 activity prevents phosphorylation-mediated inactivation of the cellular eIF2α, which is essential for initiation of cap-dependent translation. Thus, PCP behaves as a proviral factor, promoting uninterrupted synthesis of viral proteins in infected cells, which is crucial for survival and proliferation of the virus.

KEYWORDS hepatitis E virus, proteases

Hepatitis E virus (HEV) is a positive-strand RNA virus that causes acute as well as chronic infection in humans, characterized by jaundice, fever, fatigue, abdominal pain, hepatomegaly, and elevation in the levels of liver enzymes such as alanine aminotransferase and aspartate aminotransferase. It is a major contributor to epidemic outbreaks of acute hepatitis in developing countries like South Asian and African countries (1). In many cases, HEV infection results in subclinical infection among healthy individuals, which is cleared by the host without any medical intervention, but chronic infection has been reported among 50% to 60% of solid organ transplant patients (2). Another remarkable feature of HEV is its ability to cause high mortality in infected pregnant women (3–5).

Editor J.-H. James Ou, University of Southern California

Address correspondence to Milan Surjit, milan@thsti.res.in.

*Present address: Chandru Subramani, Department of Pathology, University of Texas Medical Branch, Galveston, Texas, USA.

The authors declare no conflict of interest.

Received 3 March 2023
Accepted 2 May 2023
Published 18 May 2023

HEV genomic RNA is 7.2 kb in length, with a 5′-7-methylguanosine cap and a 3′ poly(A) tail. It is divided into 8 genotypes. All genotypes encode three open reading frames (ORFs) called ORF1, ORF2, and ORF3. Genotype 1 HEV (g1-HEV) encodes a fourth ORF named ORF4 (6). ORF1 encodes a polyprotein, which may be proteolytically processed into different functional domains such as the methyltransferase, Y domain, papain-like cysteine protease (PCP), V domain, X domain, helicase, and RNA-dependent RNA polymerase (RdRp). No consensus exists regarding processing of the ORF1 polypeptide into smaller subunits in HEV-infected cells and *in vitro* (7–12). In recent studies, wheat germ cell-free expression system-mediated *in vitro*-translated ORF1 polypeptide did not show any processing of ORF1 into smaller subunits, and expression of the HEV replicon with tagged ORF1 polypeptide in mammalian cells did not show any processing of ORF1 into smaller subunits (13, 14). Nevertheless, some functional domains of ORF1 have been well characterized. Methyltransferase is involved in the 5′ capping of the viral RNA (15). Methyltransferase interacts with the X domain, and this interaction may play a role in modulating methyltransferase activity (16). The Y domain overlaps the methyltransferase and spans from 216 to 442 amino acids (aa) in ORF1. Sequence analysis suggests it to be an extension of the methyltransferase. *In silico* studies have shown the presence of a palmitoylation site in the Y domain. Site-directed mutagenesis studies have shown that 336th and 337th cysteine and 413th tryptophan residues in the Y domain are critical for viral replication (17, 18). The X domain of HEV belongs to the macrodomain family of proteins (19). It shows ADP-ribose-1′-monophosphatase activity (20). It inhibits the phosphorylation of IRF3, which is a key step in the activation of the type 1 interferon (IFN) pathway (21). HEV encodes a papain-like cysteine protease (PCP), which may be involved in ORF1 protein processing, although no clear evidence exists to support this claim. AlphaFold2-mediated *in silico* modeling of ORF1 polypeptide did not produce any domain corresponding to protease (13). In mammalian cell-based assays, PCP deubiquitinates RIG-I, TBK-1, IFN-stimulated gene 15 (ISG15), and Nedd8, indicating its ability to interfere with the host immune response pathways (22). Mutations in Cys and His amino acids of PCP abolish HEV replication, indicating an essential role of the PCP in the life cycle of HEV (10). HEV ORF1 also contains a hypervariable region between the PCP and the X domain, which is rich in proline residues. Although its exact function is not well defined, it has been shown to be a hot spot for insertion of host sequences such as the ribosomal S17 insertion (23, 24). It has been proposed to play a role in efficient replication of HEV *in vivo* (25, 26). HEV helicase possesses RNA duplex-unwinding activity and RNA 5′-triphosphatase activity (27–29). RNA-dependent RNA polymerase (RdRp) is the major component responsible for viral replication.

Both ORF2 and ORF3 proteins are translated from 2.2-kb subgenomic bicistronic RNA (30). ORF2 is the major capsid protein, and it contains a signal sequence at its N terminus, which targets it to the endoplasmic reticulum. ORF2 induces endoplasmic reticulum (ER) stress and exploits the ER-associated degradation (ERAD) pathway to get retro-translocated to the cytosol (31). ORF2 has also been shown to inhibit the NF-κB and the RIG-I signaling pathways in mammalian cell lines (32, 33). ORF3 is a small phosphoprotein that acts as a viroporin to facilitate release of the virus (34). The interaction between ORF3 and host tumor susceptibility gene 101 (TSG101) has also been shown to be essential for release of the virus (35, 36). ORF3 also downregulates Toll-like receptor 3 (TLR3)-mediated signaling in A549 cells (37). ORF4 is produced only in g1-HEV-infected cells. It plays an essential role in the replication of g1-HEV (6).

In response to viral infections, several host defense mechanisms are initiated, one of the most common being phosphorylation-mediated inactivation of the eukaryotic initiation factor 2α (eIF2α), leading to shutdown of global protein synthesis. eIF2α is inactivated by phosphorylation of its serine 51 (S51) residue by four cellular kinases, eIF2AK1 (HRI) (activated by heme deprivation), eIF2AK2 (PKR) (activated by double-stranded RNA [dsRNA]), eIF2AK3/PERK (activated by ER stress), and eIF2AK4 (GCN2) (activated by amino acid deprivation, UV rays, and some viral RNA). These four kinases are the key regulators of the cellular integrated stress response machinery (38). Although most viruses do activate one or more of the above-described four kinases, at the same time, the majority of them are also equipped with a counterstrategy to neutralize the host response. Notable examples include PKR

inhibition by NS1 of the influenza virus, PERK inhibition by the herpes simplex virus 1, and GCN2 cleavage by the human immunodeficiency virus type 1 (HIV-1) proteases (39–41).

An earlier study conducted in our laboratory constructed the host-virus protein interaction network of HEV by identifying the host interaction partners of all HEV proteins (11). Five host proteins were found to interact with the g1-HEV PCP, including eukaryotic elongation factor 1 alpha 1 (eEF1A1), eukaryotic initiation factor 2 alpha kinase 4 (eIF2AK4), protocadherin 8 (PCDH8), ring finger protein 168 (RNF168), and solute carrier family 22 member 12 (SLC22A12). Coimmunoprecipitation (co-IP) assays confirmed the interaction between PCP, eEF1A1, and eIF2AK4. Pulldown assays revealed the presence of PCP and eEF1A1 in the RdRp-associated protein complex (putative replication complex of the virus), whereas eIF2AK4 was not detected in that complex. Small interfering RNA (siRNA)-mediated ablation of eEF1A1 significantly reduced viral replication, but ablation of eIF2AK4 did not affect viral replication. Analysis of the eIF2AK4 protein sequence revealed that PCP interaction with the eIF2AK4 was mediated via the carboxy-terminal domain (CTD) of the latter. It is known that self-association of the CTD of eIF2AK4 is essential for its activity (42, 43). eIF2AK4 is also known to inhibit the replication of many RNA viruses, including the Sindbis virus (41, 44). In view of the above-described observations and considering the fact that eIF2AK4 is a key component of the integrated stress response machinery, we hypothesized that the PCP-eIF2AK4 interaction is important for HEV pathogenesis. Therefore, the current study was designed to explore the possible functional significance of the interaction between the HEV PCP and the cellular eIF2AK4.

RESULTS

The HEV PCP protein prevents eIF2AK4-mediated phosphorylation of eIF2α. eIF2AK4 phosphorylates eIF2α under conditions of nutritional stress, leading to shutdown of translation. Rapamycin treatment also induces eIF2AK4-mediated phosphorylation of eIF2α at the S51 position (45). In order to evaluate the effect of HEV PCP on eIF2AK4, we first tested whether eIF2α phosphorylation is controlled by eIF2AK4 in rapamycin-treated Huh7 cells. In agreement with earlier reports, rapamycin treatment induced eIF2α phosphorylation in Huh7 cells (Fig. 1A, top). There was no change in the level of total eIF2α (Fig. 1A, bottom). An siRNA against eIF2AK4 was used to confirm the above-described observation. eIF2AK4 siRNA was the same as described in our early report (11). A 72-h treatment with the eIF2AK4 siRNA abolished the eIF2AK4 protein in the Huh7 cells (Fig. 1B, top). The GAPDH (glyceraldehyde-3-phosphate dehydrogenase) level was measured to ensure equal loading of the samples (Fig. 1B, bottom). As expected, rapamycin treatment of eIF2AK4 siRNA-treated cells did not induce eIF2α phosphorylation, confirming that rapamycin-induced eIF2α phosphorylation was mediated by eIF2AK4 (Fig. 1A). Next, Huh7 cells were transfected with the Flag-tagged PCP expression plasmid, followed by rapamycin treatment and measurement of phospho-eIF2α level. A significant reduction in phospho-eIF2α level was observed (Fig. 1C). The total eIF2α level was unchanged in these cells (Fig. 1C, middle). PCP-Flag expression was monitored in aliquots of samples (Fig. 1C, bottom). Next, we tested if HEV infection induced a similar effect. Capped genomic RNA of genotype 1 HEV (g1-HEV) was *in vitro* synthesized, followed by transfection into Huh7 cells. Seventy-two hours post-transfection, cells were treated with rapamycin for 1 or 2 h, and the level of phospho-eIF2α or total eIF2α was monitored. There was a marked reduction in the level of phospho-eIF2α in g1-HEV-expressing cells (Fig. 1D).

PCP is a part of the ORF1 polypeptide of HEV, which also contains other nonstructural proteins of the virus, such as helicase, methyltransferase, and RNA-dependent RNA polymerase. Some reports suggest partial processing or no processing of the ORF1 polypeptide into smaller subunits in HEV-infected cells and *in vitro* (7–10, 12–14). In our earlier study, heterologous expression of ORF1 in Huh7 cells led to production of full-length polypeptide as well as partially processed peptides (11). Since the full-length ORF1 polypeptide also contains the PCP region, we tested its ability to associate with eIF2AK4. Immunoprecipitation of Flag-tagged ORF1-expressing Huh7 cell lysate (untreated or treated with rapamycin), followed by Western blot analysis using eIF2AK4 antibody, demonstrated the interaction between

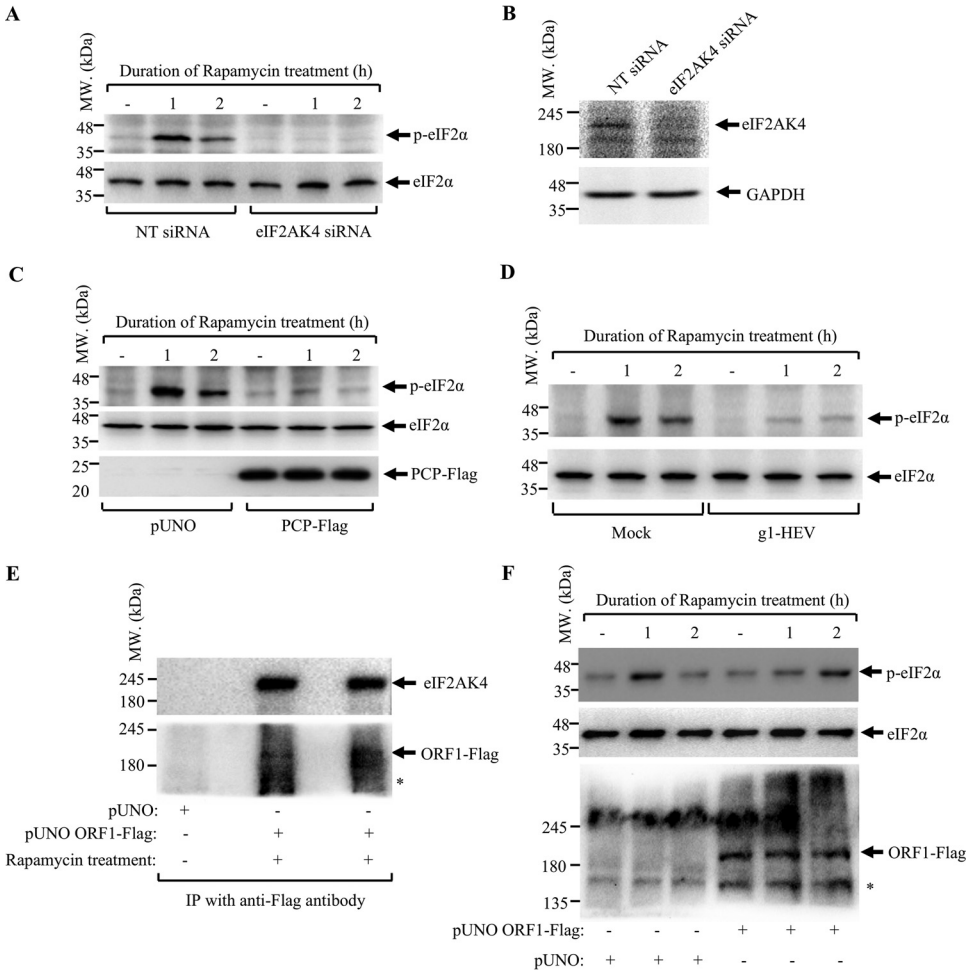

FIG 1 HEV PCP protein inhibits the activity of the host eIF2AK4 and prevents phosphorylation of the eIF2α. (A) Anti-phospho-eIF2α (top) and anti-total eIF2α (bottom) Western blotting of Huh7 cells transfected with the nontarget siRNA (NT) or eIF2AK4 siRNA and treated with 1 μM rapamycin, as indicated. (B) Anti-eIF2AK4 (top) and anti-GAPDH (bottom) Western blotting of Huh7 cells transfected for 72 h with the NT siRNA or eIF2AK4 siRNA. (C) Anti-phospho-eIF2α (top), anti-total eIF2α (middle), and anti-Flag (bottom) Western blotting of Huh7 cells transfected with the vector (pUNO) or PCP-Flag and treated with 1 μM rapamycin, as indicated. (D) Anti-phospho-eIF2α (top) and anti-total eIF2α (bottom) Western blotting of Huh7 cells mock transfected or transfected with the *in vitro*-transcribed capped g1-HEV genomic RNA and treated with1 μM rapamycin, as indicated. (E) Anti-eIF2AK4 (top) and anti-Flag (bottom) Western blotting of Huh7 cells transfected with the vector (pUNO) or ORF1-Flag and treated with 1 μM rapamycin, as indicated. (F) Anti-phospho-eIF2α (top), anti-total eIF2α (middle), and anti-Flag (bottom) Western blotting of Huh7 cells transfected with the vector (pUNO) or ORF1-Flag, as indicated. *, nonspecific band. Images are representative of three independent experiments.

ORF1 and eIF2AK4 (Fig. 1E, top). Aliquots of the samples were used to detect the expression of ORF1 (Fig. 1E, bottom). Although full-length ORF1 polypeptide was clearly detected, no clear band indicative of partially processed ORF1 polypeptide was detected (Fig. 1E, bottom). Next, Huh7 cells were transfected with the Flag-tagged ORF1 expression plasmid, followed by rapamycin treatment and measurement of phospho-eIF2α level. A significant reduction in phospho-eIF2α level was observed upon 1 h treatment with rapamycin; however, its level was increased at the 2-h time point in ORF1-expressing cells (Fig. 1F, top). Since the effect of rapamycin on eIF2AK4 activity is short-lived, the increase in eIF2α phosphorylation at 2 h could be due to the effect of other proteins produced from the ORF1 polypeptide. The total eIF2α level was unchanged in these cells (Fig. 1F, middle). ORF1-Flag expression was monitored in aliquots of samples (Fig. 1F, bottom).

Next, an *in vitro* phosphorylation assay was performed to check the effect of PCP on eIF2AK4-mediated phosphorylation of purified recombinant eIF2α. PCP was purified from Huh7 cells expressing the PCP-Flag protein (Fig. 2A). Purified recombinant eIF2α was obtained from a commercial supplier (Fig. 2B). eIF2AK4 was immunoprecipitated from the Huh7 cells

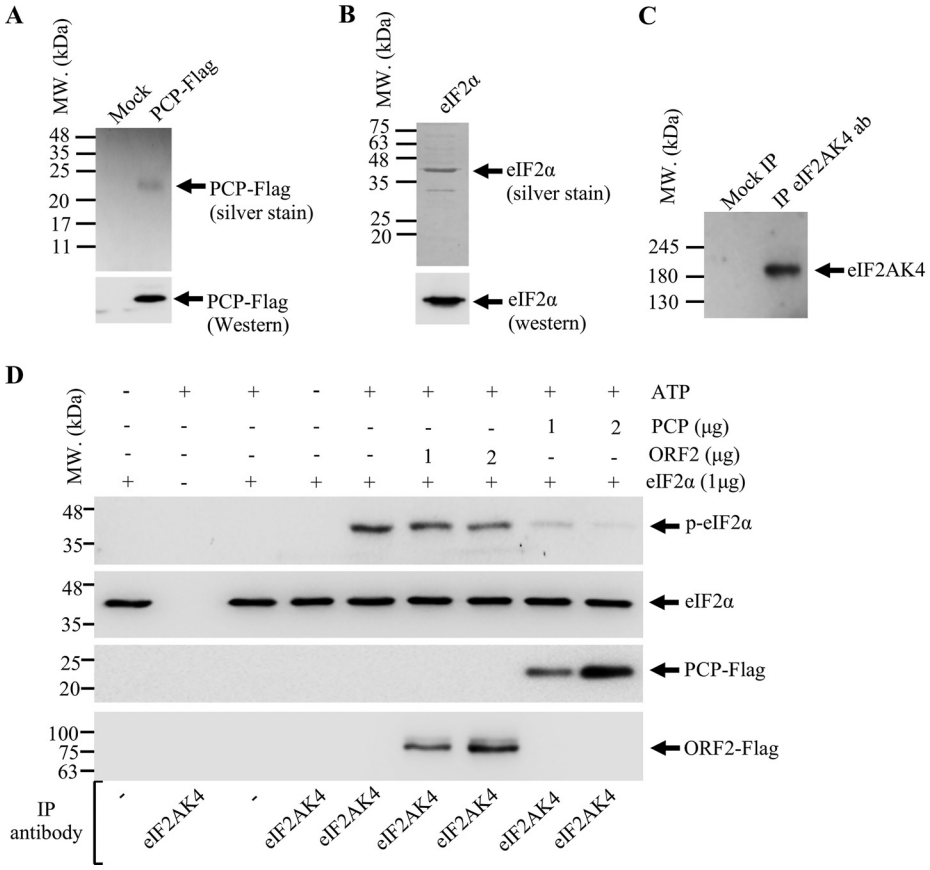

FIG 2 HEV PCP protein inhibits eIF2α phosphorylation *in vitro*. (A) Mock or PCP-Flag-expressing Huh7 cell lysate was immunoprecipitated using Flag agarose beads, followed by silver staining (top) or Western blotting using anti-Flag antibody (bottom). (B) *E. coli*-purified eIF2α was silver stained (top) or Western blotted using anti-eIF2α antibody (bottom) (C) Endogenous eIF2AK4 protein was immunoprecipitated from Huh7 cells using anti-eIF2AK4 antibody or protein G-agarose only (mock), followed by Western blotting using anti-eIF2AK4 antibody. (D) *E. coli*-purified eIF2α was *in vitro* phosphorylated in the presence of eIF2AK4, PCP, and ORF2 proteins, as indicated, followed by Western blotting of aliquots of the samples using antibodies against p-eIF2α (S51, 1st panel), eIF2α (2nd panel), and Flag (3rd and 4th panels). Images in panels A to C are representative of one experiment, and the image in panel D is representative of two independent experiments.

(Fig. 2C). Purified recombinant ORF2 (Flag tagged) was used as a control to monitor specificity of the effect of PCP. *In vitro* phosphorylation of eIF2α by eIF2AK4 demonstrated a significant reduction in the level of phospho-eIF2α in the presence of PCP (Fig. 2D). The presence of ORF2 protein had no effect on the level of phospho-eIF2α (Fig. 2D). Collectively, these results confirm that HEV PCP inhibits the activity of eIF2AK4.

Deletion and point mutation analyses of HEV PCP protein to identify the amino acids essential for its interaction with the eIF2AK4. In order to demonstrate if the PCP-eIF2AK4 interaction was responsible for inhibition of the eIF2AK4 activity by PCP, we started with characterizing the interaction between PCP and eIF2AK4 by the yeast two-hybrid (Y2H) assay. The Y2H library clone of eIF2AK4, which interacts with PCP, contains only the C-terminal domain (1537 to 1659 aa) of eIF2AK4 (Fig. 3A). Overlapping deletions of PCP were cloned into the pGBKT7 vector and GAL4-based Y2H assay was carried out (Fig. 3B). The Y2H Gold strain was cotransformed with the AD eIF2AK4-CTD (eIF2AK4-CTD in the pGADT7 vector) and BD PCP deletions (PCP deletions in the pGBKT7 vector), followed by selection of cotransformants on LT$^-$, LTHA$^-$, LTH-aureobasidin A (A^{r+}), LT$^-$ plus X-alpha-galactosidase (X-α-gal), and LTH$^-$ plus 5 to 30 mM 3-amino-1,2,4-triazole (3-AT)-supplemented plates (Fig. 3B). Y2H Gold contains four independent reporter genes to monitor protein-protein interaction: the *HIS3* gene allows the growth on histidine (H$^-$) auxotrophic plates, the *ADE2* gene allows the growth on adenine (A$^-$) auxotrophic plates, the *MEL1* gene converts X-α-gal substrate into blue-colored product, and the *AUR1-C* gene confers resistance to aureobasidin A (A^{r+}). Stringency of His reporter activity was controlled by

A

B

	Schematic of PCP deletions and mutations	LT$^-$	LTHA$^-$	LTH$^-$ A^{r+}	LT$^-$ + X-α gal	LTH$^-$ + 3AT(mM)				
						0	5	10	20	30
AD eIF2AK4-CTD + BD PCP (1-161aa)	1 161aa	+++	+++	+++	+	+++	+++	+++	+++	++
AD eIF2AK4-CTD + BD PCP (1-70aa)	1 70aa	+++	+++	+++	++	+++	+++	+++	+++	++
AD eIF2AK4-CTD + BD PCP (1-102aa)	1 102aa	+++	+++	+++	++	+++	+++	+++	+++	++
AD eIF2AK4-CTD + BD PCP (1-120aa)	1 120aa	+++	+++	+++	++	+++	+++	+++	+++	++
AD eIF2AK4-CTD + BD PCP (70-161aa)	70 161aa	+++	−	−	−	+	−	−	−	−
AD eIF2AK4-CTD + BD PCP (90-161aa)	90 161aa	+++	−	−	−	−	−	−	−	−
AD eIF2AK4-CTD + BD PCP (39-96aa)	39 96aa	+++	+++	+++	++	+++	+++	++	+++	++
AD eIF2AK4-CTD + BD PCP(39-57aa)	39 57aa	+++	+++	+++	++	+++	+++	+++	+++	++
AD eIF2AK4-CTD + BD PCP A57F	A57F 1 161aa	+++	+++	+++	++	+++	+++	+++	++	+
AD eIF2AK4-CTD + BD PCP F53A	F53A 1 161aa	+++	−	−	+	+	−	−	−	−
AD eIF2AK4-CTD + BD PCP E58A	E58A 1 161aa	+++	+++	+++	++	+++	+++	+++	++	+
AD eIF2AK4-CTD + BD PCP F53A.E58A	F53A E58A 1 161aa	+++	+	+	+	+	−	−	−	−
AD eIF2AK4-CTD + BD PCP C50A	C50A 1 161aa	+++	++	+++	+++	+++	++	+	−	−
AD eIF2AK4-CTD + BD PCP C52A	C52A 1 161aa	+++	+++	+++	+++	+++	+++	++	+	−
AD eIF2AK4-CTD + BD		+++	−	++	+	++	−	−	−	−
AD + BD PCP (1-161aa)	1 161aa	+++	−	−	−	−	−	−	−	−

C

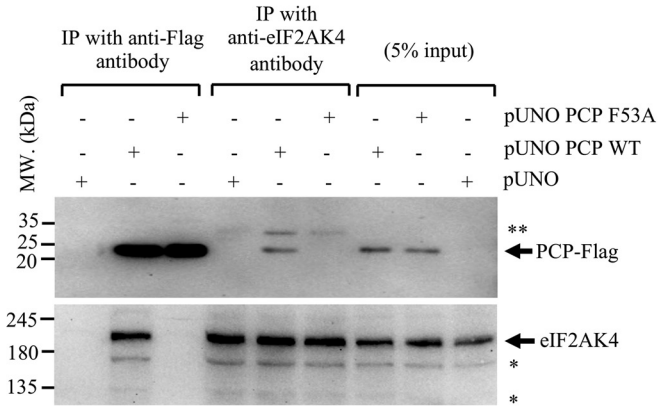

FIG 3 Deletion and point mutation analyses of the HEV PCP and eIF2AK4 interaction. (A) Schematic representation of the eIF2AK4 protein domains (RWD, YKD, KD, HisRS-like domain, and CTD). Amino acid (aa) positions are indicated against each domain. (B) Results of Y2H analysis of the interaction of PCP deletion and point mutants with the eIF2AK4-CTD. AD eIF2AK4-CTD, eIF2AK4-CTD cloned downstream of the GAL4 activation domain coding sequence. BD PCP (1 to 161 aa), 1 to 161 aa (PCP WT) of PCP cloned downstream of the GAL4 BD. Different deletion or point mutations of PCP are denoted similarly. Lengths of the retained amino acid sequence in the deletion mutants are graphically represented as solid lines. The "T" mark on full-length PCP represents the point mutation incorporated. + + +, strong growth; + +, moderate growth; +, poor growth; −, no growth; L, leucine; T, tryptophan; H, histidine; A, adenine hemisulfate; A^{r+}, aureobasidin; 3-AT, 3-amino-1,2,4-triazole; −, deficiency in the medium; +, supplemented in the medium. (C) Anti-Flag (top) and anti-eIF2AK4 Western blotting of indicated samples immunoprecipitated with the anti-Flag or anti-eIF2AK4 antibody. Five percent input denotes 5% of the total cell extract used in the immunoprecipitation. * and **, nonspecific bands. The image in panel B is representative of three independent experiments, and the image in panel C is representative of three independent experiments.

adding increasing concentrations (5, 10, 20, and 30 mM) of 3AT to LTH$^-$ plates. Full-length PCP (1 to 161 aa) and the CTD domain of eIF2AK4 (1537 to 1659 aa) cotransformants activated all four reporter genes and showed strong growth on LTHA$^-$ and LTH-A^{r+} plates and produced blue-colored colonies on X-α-gal-supplemented plates (Fig. 3B). Note that +++, ++, and + represent strong, moderate, and weak growth/color, respectively. PCP

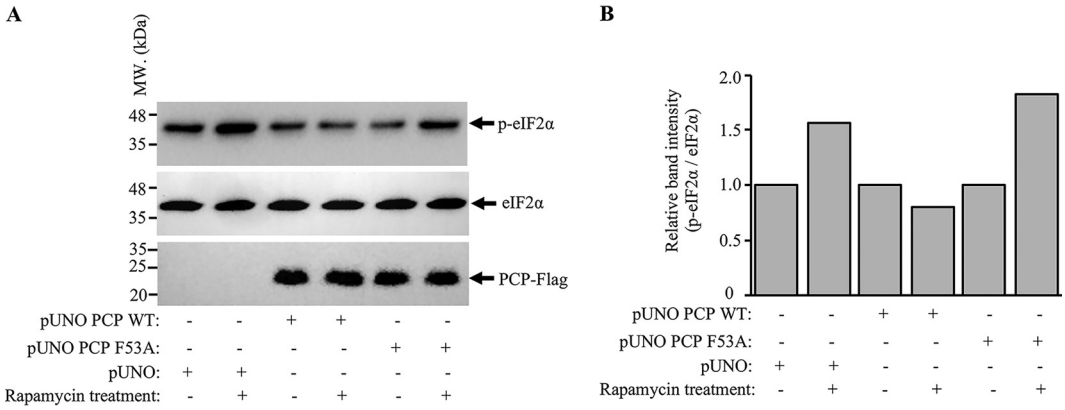

FIG 4 The F53A PCP mutant is unable to inhibit rapamycin-induced phosphorylation of eIF2α. (A) Anti-phospho-eIF2α (top), anti-total eIF2α (middle), and anti-Flag (bottom) Western blotting of Huh7 cells transfected with the vector (pUNO) or WT PCP-Flag or F53A PCP-Flag mutant and treated with 1 μM rapamycin, as indicated. (B) Graph showing densitometry-based quantification of band intensities of phospho-eIF2α (normalized to that of total eIF2α) shown in panel A. Values obtained for phospho-eIF2α were divided by that of total eIF2α; the ratio thus obtained was considered one for the untreated samples, and corresponding values in rapamycin-treated samples were calculated with respect to that. Values are the average of duplicate readings. The image in panel A is representative of two independent experiments. In panel B, the graph shows the mean band intensity of two independent blots.

and eIF2AK4 interaction displayed growth up to 30 mM 3-AT on the LTH$^-$ plates (Fig. 3B). Out of the different deletions, 1 to 120 aa, 1 to 102 aa,1 to 70 aa, 39 to 57 aa, and 39 to 96 aa of PCP showed interaction with eIF2AK4 (Fig. 3B). Therefore, 39 to 57 aa is the minimal region of PCP that interacts with the eIF2AK4.

Next, we analyzed the predicted secondary structure of the PCP protein using the MacVector software (MacVector, Inc., USA) to further characterize the motif in PCP that interacts with eIF2AK4. PCP secondary structure analysis revealed the presence of a β-sheet between the 51st to 54th aa within the 39- to 57-aa interaction domain. Mutating F53 to A completely abrogated the β-sheet, whereas mutating A57 to F or E58 to A marginally decreased or further expanded the β-sheet, respectively. Between the 50th and 54th aa of PCP, two cysteine residues (C50, C52; corresponds to C481 and C483 in the ORF1) are present, which have been shown to be crucial for HEV replication (10). C50A or C52A mutations completely abrogated the β-sheet, as seen in the case of the F53A mutant. Effect of these mutations on the interaction of PCP with eIF2AK4 was evaluated by the Y2H assay. The PCP F53A mutant did not interact with the eIF2AK4, whereas the PCP A57F mutant and PCP E58A mutant interacted with the eIF2AK4 like the wild-type (WT) PCP (Fig. 3B). As expected, the PCP F53A E58A double mutant did not interact with eIF2AK4 (Fig. 3B). Interestingly, the PCP-eIF2AK4 interaction was not affected by the C50A and C52A mutations (Fig. 3B).

Next, a coimmunoprecipitation assay was performed to confirm the observation of the Y2H assay. The F53A mutant PCP was cloned into the pUNO mammalian expression vector. Huh7 cells were transfected with either pUNO vector or PCP WT or PCP F53A mutant expression plasmids, followed by immunoprecipitation of the whole-cell extract using anti-Flag or anti-eIF2AK4 antibody. Aliquots of the immunoprecipitated samples were subjected to Western blotting using anti-Flag or anti-eIF2AK4 antibody. Anti-Flag and anti-eIF2AK4 antibodies could pull down eIF2AK4 or PCP proteins, respectively, in WT PCP-expressing cells (Fig. 3C). However, the same antibodies could not pull down eIF2AK4 or PCP proteins in PCP F53A-expressing cells (Fig. 3C). Five percent of the whole-cell lysate was used as input to ensure that both proteins are expressed in the respective cells (Fig. 3C).

The HEV F53A PCP mutant loses the ability to inhibit rapamycin-induced eIF2α phosphorylation. Since F53A PCP mutant could not interact with eIF2AK4, we tested whether this mutant retains the ability to inhibit rapamycin-induced eIF2α phosphorylation. Whole-cell extract was prepared from Huh7 cells transfected with empty vector (pUNO), WT PCP, or F53A PCP mutant, followed by 1 h treatment with rapamycin and subjected to Western blot analysis using anti-phospho-eIF2α antibody. As shown earlier, rapamycin treatment increased phospho-eIF2α levels in cells transfected with pUNO, and there was no change in its level in cells expressing PCP WT (Fig. 4A, top). There was an increase in

phospho-eIF2α level in cells expressing the F53A PCP mutant upon treatment with rapamycin, suggesting that F53A mutation abolishes the ability of PCP to inhibit rapamycin-induced eIF2α phosphorylation (Fig. 4A, top). Total eIF2α and PCP levels were monitored in aliquots of the same sample to ensure equal loading of protein across the samples and equal expression of wild-type and mutant PCP proteins, respectively (Fig. 4A, middle and bottom). Densitometry-based quantification of band intensities of phospho-eIF2α (normalized to that of total eIF2α) is shown in Fig. 4B. Note that in Fig. 4B, values of untreated samples have been considered 1, and changes in band intensity in rapamycin-treated samples were calculated with respect to that.

HEV PCP inhibits dimerization of the eIF2AK4-CTD. Dimerization of eIF2AK4 is essential for its function, and the CTD of eIF2AK4 self-associates to form the dimer. Since PCP interacts with the CTD of eIF2AK4, the effect of PCP on eIF2AK4 dimerization was measured by a glutathione *S*-transferase (GST) pulldown assay. eIF2AK4-CTD was expressed as GST and His-tagged fusion proteins in *Escherichia coli*. Glutathione agarose and nickel-nitrilotriacetic acid (NTA) affinity purification showed the presence of eIF2AK4-CTD protein in the eluate (Fig. 5A and B). Western blotting using anti-GST and anti-His antibodies confirmed the presence of proteins in the respective elution fractions (Fig. 5A and B). The wild type and F53A mutant PCP protein were purified from mammalian cells by Flag affinity purification (Fig. 5C). Recombinant His-ORF2 purified from *Pichia pastoris* was used as a control to monitor specificity of the interaction between the His-eIF2AK4-CTD and the GST-eIF2AK4-CTD (46). Glutathione agarose-bound GST-eIF2AK4-CTD was incubated with the His-eIF2AK4-CTD or His-ORF2, and bound proteins were eluted using glutathione, followed by Western blot analysis of aliquots of the eluted samples using anti-GST and anti-His antibody. Only His-eIF2AK4-CTD could bind to the GST-eIF2AK4-CTD, demonstrating their self-association (Fig. 5D, top and middle). An aliquot of the samples was visualized using Coomassie brilliant blue staining, which showed similar results (Fig. 5D, bottom). Ten percent of the samples used for pulldown assay was loaded in parallel to show the amount of input samples (input, 10%) (Fig. 5D).

Next, a GST pulldown assay was performed in the presence of increasing amount of wild type and F53A mutant PCP protein. The addition of 1 μg wild-type PCP protein had no effect on self-association of eIF2AK4-CTD (Fig. 5E). However, addition of 5 μg or 10 μg of WT PCP protein significantly reduced or completely abolished the interaction between GST-eIF2AK4-CTD and His-eIF2AK4-CTD, respectively (Fig. 5E, first panel). In contrast, F53A mutant PCP protein did not affect the interaction between GST-eIF2AK4-CTD and His-eIF2AK4-CTD under the tested conditions. Wild-type PCP was bound to GST-eIF2AK4-CTD at 5- and 10-μg quantities (Fig. 5E, second panel). Anti-GST Western blot analysis demonstrated the presence of GST or GST-eIF2AK4-CTD protein in the pulldown samples (Fig. 5E, third panel). The fourth panel shows Coomassie brilliant blue staining of aliquots of the same samples (Fig. 5E, fourth panel).

Effect of the F53A mutation in the PCP on the HEV replication. In order to evaluate the functional significance of the PCP-eIF2AK4 interaction on the HEV replication, we introduced F53A mutation in the g1-HEV genome. *In vitro*-transcribed capped wild-type or F53A mutant PCP g1-HEV genomic RNA was transfected into the ORF4-Huh7 cells, followed by measurement of viral replication by immunofluorescence visualization of the viral helicase and ORF2 proteins and quantitative real-time PCR (qRT-PCR) measurement of intracellular levels of viral RNA. Note that our earlier study has shown that ORF4-Huh7 cells support efficient replication of g1-HEV (6, 47). There was a significant reduction in both helicase and ORF2-positive cells in the F53A mutant PCP-expressing cells (Fig. 6A and B). qRT-PCR analysis of the viral RNA level showed a similar pattern (Fig. 6C).

An earlier study has shown that PCP inhibits the RIG-I signaling pathway, leading to inhibition of host antiviral response (22). Therefore, it is probable that the poor replication of the F53A PCP mutant virus is attributed to its inability to inhibit the host RIG-I signaling pathway. To test this, a constitutively active mutant of RIG-I, R-C (harboring only the CARD domains), was used. R-C signaling-dependent activation of the IFN-β promoter was evaluated in the WT PCP and F53A mutant PCP-expressing cells (Fig. 6D). Both WT PCP and F53A mutant PCP could inhibit R-C-induced activation of the IFN-β promoter, indicating that F53A mutant PCP retains the ability to inhibit the RIG-I signaling pathway. This suggests

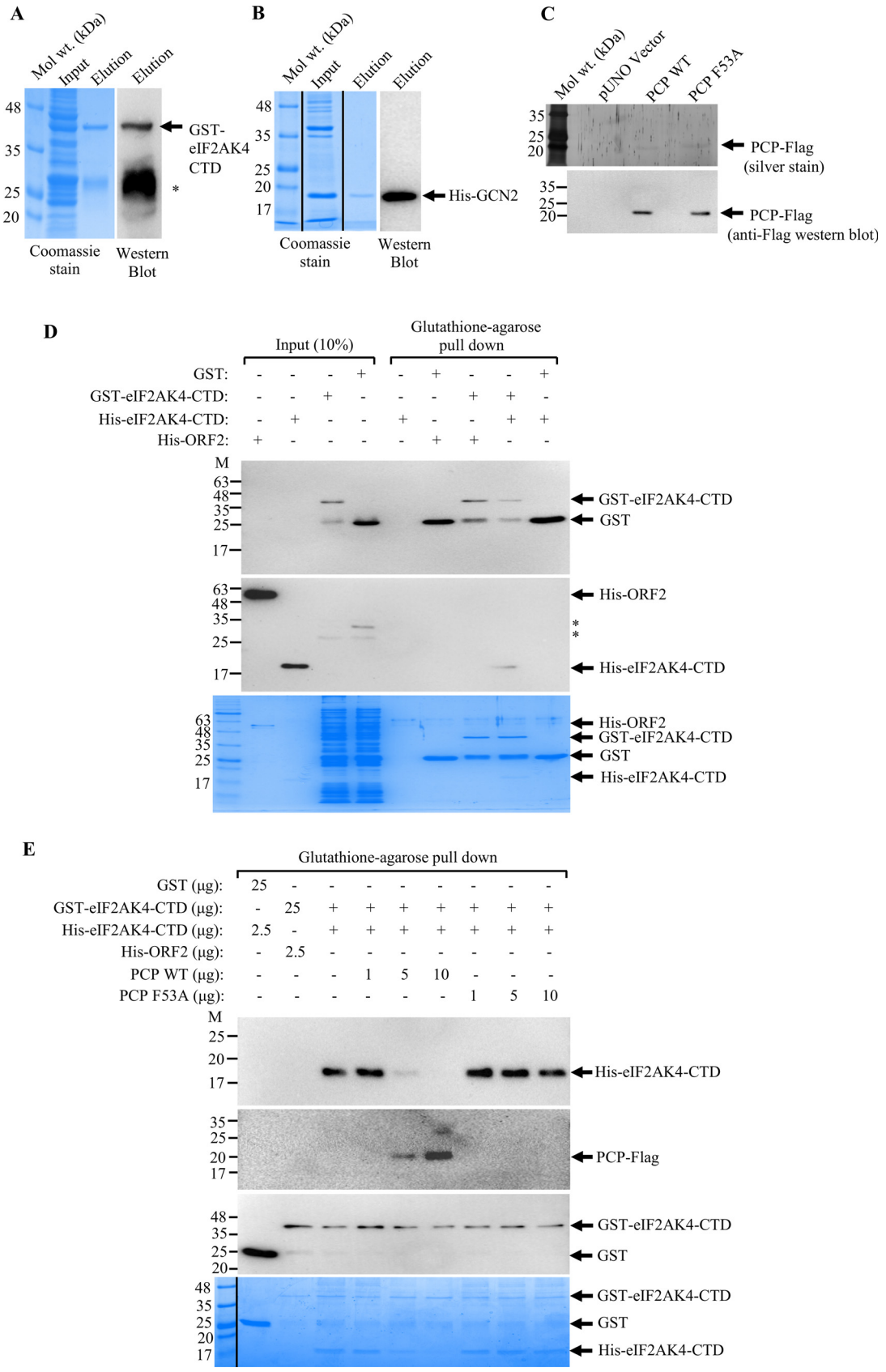

FIG 5 PCP inhibits self-association of the eIF2AK4-CTD. (A) Coomassie staining (left) and anti-GST Western blotting (right) showing recombinant purified GST-eIF2AK4-CTD. (B) Coomassie staining (left) and anti-His (right) Western blotting showing

(Continued on next page)

that the poor replication of g1-HEV expressing the F53A mutant PCP is likely attributed to its inability to bind to eIF2AK4. Taken together, these results demonstrate that PCP-mediated inhibition of the eIF2AK4 activity is important for efficient replication of the g1-HEV.

DISCUSSION

An earlier study from our laboratory reported the virus-host protein interaction network of the HEV (11). One of the remarkable finding of the study was identification of the interaction between the HEV PCP and the cellular eIF2AK4 protein. Through pulldown assays using HEV-RdRp or HEV-ORF4 proteins as baits, we showed HEV PCP to be a component of the putative viral replication complex (RdRp-associated protein complex). However, eIF2AK4 was not detected in the same complex, suggesting that eIF2AK4-PCP interaction may have an independent function in the life cycle of HEV. Here, we show the ability of the PCP to inhibit the activity of the eIF2AK4 and evaluate the functional importance of the interaction.

Viruses are known to hijack the cellular translation machinery to favor the synthesis of their own proteins and to control their own gene expression machinery, which ultimately lead to increased viral replication. Since cellular translation is tightly controlled by the cellular stress sensors, in order to become a successful pathogen, viruses adopt various strategies to modulate the host stress response pathways to favor viral translation. Four key cellular enzymes control the integrated stress response pathway, which is fundamental to survival of a cell under different conditions of stress. These include eIF2AK1 (HRI), eIF2AK2 (PKR), eIF2AK3 (PERK), and eIF2AK4 (GCN2). Upon stress sensing, these enzymes are activated and phosphorylate the serine 51 residue of the eukaryotic initiation factor 2α (eIF2α), resulting in shutdown of cap-dependent translation. Iron deficiency is sensed by eIF2AK1, double-stranded RNA is sensed by eIF2AK2, ER stress is sensed by the eIF2AK3, and amino acid deficiency or UV radiation is sensed by eIF2AK4 (38). eIF2AK4 is also activated by many RNA viruses, including the Sindbis virus, poliovirus, and human immunodeficiency virus type 1 (HIV-1). It exerts an antiviral role by inhibiting the viral translation in the infected cells (44). Since viral infection activates one or more of the above-mentioned kinases, viruses have evolved numerous strategies to antagonize the function of those kinases. For example, Rift Valley fever virus degrades PKR (48). The TRS1 protein of human cytomegalovirus 1 (HCMV2) binds to PKR and HRI and inhibits their activity (49, 50). HIV-1 protease antagonizes the eIF2AK4 activity by proteolytically cleaving it (41). Vaccinia virus (VV) K3L protein interacts with the catalytic domain of the eIF2AK4 and inhibits its function (51). HEV seems to have evolved an analogous mechanism to antagonize the function of eIF2AK4 in the infected cells, as evident from our current study.

eIF2AK4 protein is evolutionary conserved from yeast to humans. It is composed of five protein domains, (i) RING finger-containing proteins, WD repeat-containing proteins, and yeast DEAD (DEXD)-like helicases (RWD), (ii) pseudokinase domain (PKD), (iii) kinase domain (KD), (iv) histidyl t-RNA synthetase-like domain involved in binding to uncharged tRNA (HisRS), and (v) C-terminal dimerization domain (CTDD) that assists in tRNA binding (52).

Dimerization of the CTD domain is essential for the activity of eIF2AK4, and our data show that PCP directly binds to and competitively inhibits CTD dimerization, leading to inactivation of eIF2AK4. Thus, HEV has evolved an ingenuous mechanism to counteract the function of eIF2AK4, thereby maintaining continuous cap-dependent translation in the infected cells. This finding adds a new characteristic to the known functions of the PCP protein as a proviral factor. It is likely that HEV-infected cells face amino acid shortage due to increased protein synthesis requirement, which activates eIF2AK4. Alternatively, eIF2AK4 might be activated by the HEV genomic RNA as an antiviral response.

FIG 5 Legend (Continued)

the His-eIF2AK4-CTD. (C) Silver staining (top) and anti-Flag Western blotting (bottom) showing the Flag antibody-purified WT PCP and F53A mutant PCP protein. (D) Anti-His (top) and anti-GST (middle) Western blotting of GST pulldown assay using different samples as indicated. Input denotes 10% of each sample aliquoted before the pulldown assay. (D, Bottom) Coomassie blue staining of aliquots of the GST pulldown assay samples. *, nonspecific bands. (E) Anti-His (top panel), anti-Flag (second panel), and anti-GST (third panel) Western blotting of GST pulldown assay using indicated samples. The fourth panel shows Coomassie blue staining of aliquots of the GST pulldown assay samples. Images in panels A to C are representative of one experiment, and images in panels D and E are representative of two independent experiments.

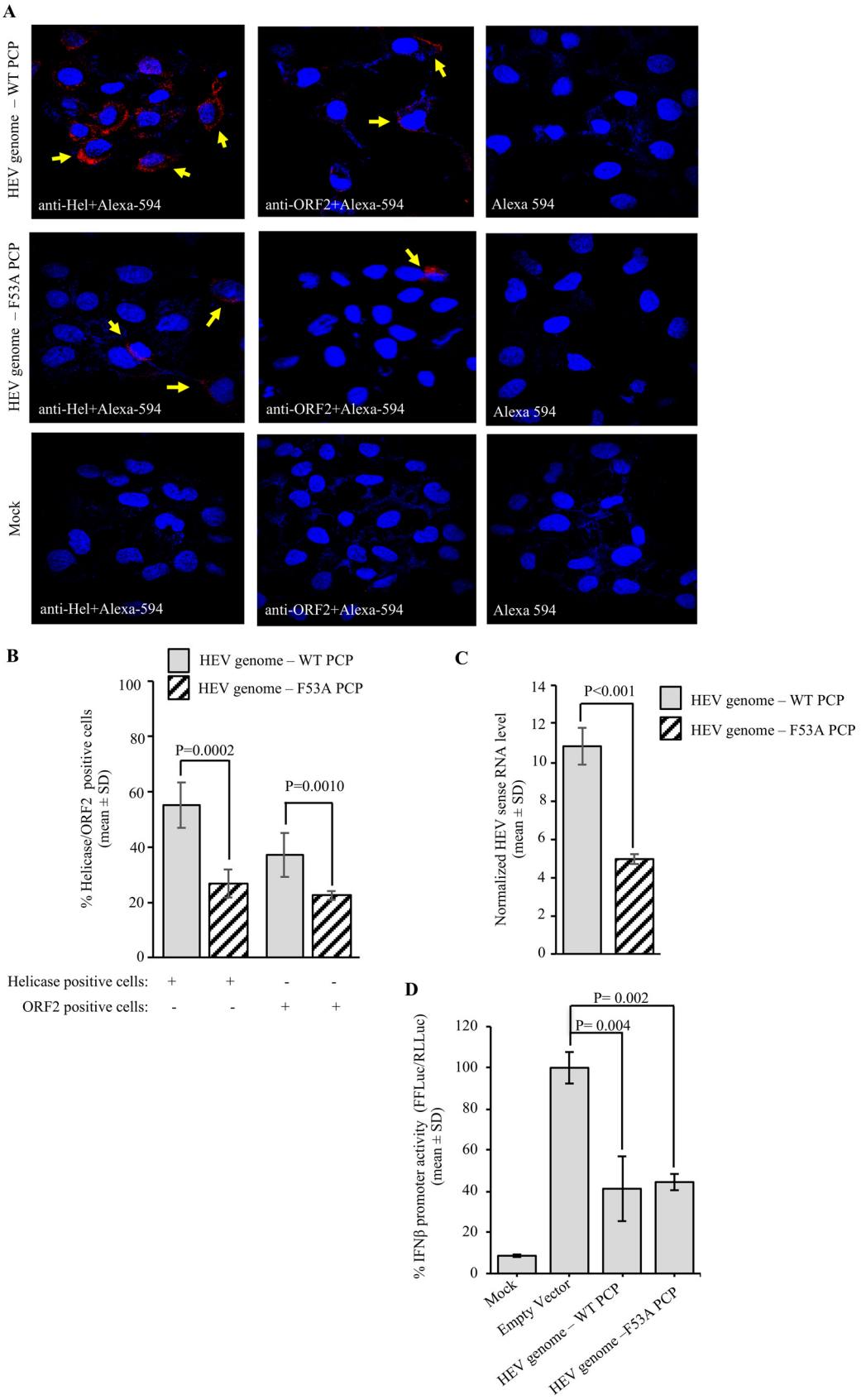

FIG 6 F53A PCP mutation reduces the rate of HEV replication in Huh7 cells. (A) Immunofluorescence images of anti-Helicase and anti-ORF2 antibody stained Huh7 cells expressing the wild type g1-HEV or F53A PCP mutant g1-HEV. Fluorescent

(Continued on next page)

The eIF2AK4 interaction domain of PCP was mapped to a 19-amino-acid (39 to 57 aa) region. This region contains the 483rd cysteine (C483) residue, which, together with the 590th histidine (H590), forms the catalytic dyad of the protease (10, 19). Site-directed mutagenesis of C483A abolishes viral replication (10). Site-directed mutagenesis of C481A, which lies within the 39- to 57-aa eIF2AK4-binding domain also abolishes viral replication (10). Both of these mutations also render the PCP catalytically inactive. In our analysis, C481A and C483A mutant PCP did not affect the interaction between PCP and eIF2AK4. In contrast, the F53A (corresponding to F484 in ORF1) mutation inhibited the interaction of PCP and ORF1 with the eIF2AK4 and reduced viral replication. Hence, it is clear that the catalytic dyad of PCP is not involved in binding to the eIF2AK4, and its effect on viral replication is likely not mediated through eIF2AK4. Also note that our results show that the F53A PCP mutant retains the ability to inhibit the RIG-I signaling pathway. Hence, the ability to inhibit the activity of eIF2AK4 is an additional characteristic of the PCP protein. Although the predicted secondary structure analysis of the F53A PCP protein indicates the loss of a β-sheet due to the mutation, the molecular mechanism by which F53A mutation disrupts the interaction between PCP-eIF2AK4 remains to be established.

Our data show that the F53A PCP mutant virus, which is unable to inhibit eIF2AK4 activity, replicates poorly in mammalian cells. Therefore, an inhibitor of PCP-eIF2AK4 interaction may prove to be a specific antiviral strategy against HEV. In summary, the current study demonstrates a proviral role of the HEV PCP by virtue of its ability to inhibit the activity of host eIF2AK4, thereby permitting uninterrupted synthesis of the viral proteins, resulting in efficient replication of HEV in the infected cells.

MATERIALS AND METHODS

Reagents, antibiotics, and antibodies. The Y2H Gold yeast strain, X-alpha-galactosidase (X-α-gal), and aureobasidin A were purchased from Clontech (CA, USA). FireScript RT cDNA synthesis kit and 5$\times$ Hot FirePol EvaGreen qPCR Mix Plus (ROX) were from Solis Biodyne (Tartu, Estonia). Pierce glutathione agarose, glutathione, mMessage mMachine T7 transcription kit, and blasticidin were from Thermo Scientific (MA, USA). Control siRNA (catalog no. SC-37007) and eIF2AK4 siRNA (catalog no. SC-45644) were from Santa Cruz Biotechnology (TX, USA). Kanamycin and ampicillin were from MP Biomedicals (CA, USA). Anti-GST antibody was from Cell Signaling Technology (MA, USA). Anti-Flag, anti-His, anti-eIF2AK4, and anti-eIF2α were from Santa Cruz Biotechnology (TX, USA); anti-rabbit Alexa Fluor 594 and Prolong Gold antifade mountant with DAPI (4′,6-diamidino-2-phenylindole) were from Sigma (MO, USA). Flag M2 agarose, Flag peptide, and 3-amino-1,2,4-triazole (3-AT) were from Sigma (MO, USA).

Plasmids. The pSK HEV2 (GenBank accession no. AF444002) plasmid containing the cDNA corresponding to the g1-HEV genome was used in all experiments (53). We considered 1,321 nucleotides from the 5′ end to 1,801 nucleotides of the g1-HEV genome to be the full-length PCP encoding region (cloned into pGAD vector [pGAD-PCP], as reported [16]). pGBK 1-120 PCP, pGBK 1-102 PCP, and pGBK 39-96 PCP were generated by PCR amplification of 1-120 PCP, 1-102 PCP, and 39-96 PCP regions using pGAD-PCP as the template (16) and the following set of primers: PCP FP (EcoRI) and 1-120 PCP RP (XhoI) for pGBK, 1-120 PCP; PCP FP (EcoRI), and 1-102 PCP RP (XhoI) for pGBK; and 1-102 PCP, 39-96 PCP FP (EcoRI), and 39-96 PCP RP (XhoI) primers for pGBK 39-96 PCP. Primer sequences are listed in Table 1. PCR products and the pGBKT7 vector were digested with EcoRI and XhoI, followed by ligation of different deletion mutants into the linearized pGBKT7 vector. pGBK 1-70 PCP was generated by digesting pGBK-PCP (11) with StuI and NotI, followed by blunting of the NotI site, gel extraction of the ~7.5-kb DNA fragment, and self-ligation. pGBK 70-161 PCP was generated by restriction digestion of the pGBK-PCP with EcoRI and StuI, blunting of the EcoRI site, gel extraction of the ~7.6-kb DNA fragment, and self-ligation. pGBK 90-161 PCP was generated by restriction digestion of the pGBK-PCP with SnaBI and NotI, followed by gel extraction of a 220-bp fragment. The pGBKT7 vector was digested with NcoI, blunted, and then digested with NotI. The linearized vector and the insert fragments were ligated to generate the pGBK 90-161 PCP. pGBK 39-57 PCP was generated by restriction digestion of the pGAD 39-96 PCP with EcoRI and PstI, followed by gel extraction of the 57-bp PCP fragment. pGBKT7 was digested with EcoRI and PstI, followed by ligation of the gel-extracted 57-bp fragment between the EcoRI and PstI sites. pGBK A57F PCP was generated as per the following method. The N-terminal domain (NTD) of PCP was PCR amplified using the pGBK-PCP template and PCP FP (EcoRI) and PCP A57F RP primers. The PCR product was

FIG 6 Legend (Continued)
positive cells are indicated by arrows. (B) Quantification of the helicase and ORF2-positive cells shown in panel A. Data are represented as mean ± SD percentage of 10 randomly selected fields. (C) qRT-PCR of HEV sense RNA level in the ORF4-Huh7 cells expressing the wild-type g1-HEV or F53A PCP mutant g1-HEV. Data are represented as mean ± SD of three independent experiments. (D) Percentage of IFN-β promoter activity in HEK 293T cells expressing the empty vector, WT PCP, or F53A PCP and coexpressing the constitutively active mutant of RIG-I, R-C, as indicated. Mock corresponds to assay with vector alone and no R-C. Image A is representative of three independent experiments. In panels B to D, data are represented as mean ± SD of three independent experiments.

TABLE 1 Primers used in this study

Primer name	Primer sequence
PCP FP (EcoRI)	5′-TGCTCAGAATTCGCTCAGTGTAGGCGCTG-3′
PCP RP (XhoI)	5′-AGACTGCTCGAGTTAGAGATTGTGGCGCTCTGG-3′
1-120 PCP RP (XhoI)	5′-CGACCTCGAGTGTGGCGGTCAGCCGGCCT-3′
1-102 PCP RP (XhoI)	5′-ATGGCTCTGAGTTGGTAAAGCGGTTGGAGGG-3′
39-96 PCP FP (EcoRI)	5′-ATGCGAATTCTTTTGCTGCTTTATGAAGTGGCTGG-3
39-96 PCP RP (XhoI)	5′-ATGCCTCGAGGGCAGTGCCAGGGACTACGTAGG-3′
PCP A57F RP	5′-CCTCGTTGTCATGGCCCTGGTCGCCAACGACGCCTTCAAAAGGTTGTAGA-3′
PCP F53A RP	5′-ATGCCTGCAGGTTGTAGAGCACAGGTGCACTCCTGGCCCAGCCA-3′
PCP E58A RP	5′-CCTCGTTGTCATGGCCCTGGTCGCCAACGACGCCAGCTGCAGGTTGT-3′
PCP F53A, E58A RP	5′-CCTCGTTGTCATGGCCCTGGTCGCCAACGACGCCAGCTGCAGGTTGT-3′
PCP C50A FP	5′-GTGGCTGGGCCAGGAGGCCACCTGTTTTCTACAACCT-3′
PCP C50A RP	5′-TTCATAAAGCAGCAAAACTTTGAGACCGCC-3′
PCP C52A FP	5′-GGGCCAGGAGTGCACCGCCTTTCTACAACCTGCAG-3′
PCP C52A RP	5′-AGCCACTTCATAAAGCAGCAAAAC-3′
hGCN2 CTD FP (EcoRI)	5′-TAGTGAATTCGGGTCATTTTCTAATGCTTCAGGTTTGTT-3′
GCN2 RP (XhoI)	5′-ATGCCTCGAGAAATAAGATTCTGTAGTAGTCATC-3′
PCP FP (AgeI)	5′-GACACCGGTCATCATGCAGTGTAGGCGCTGGCTCTC -3′
PCP Flag RP (NheI)	5′-GACGCTAGCTCACTTATCGTCATCGTCCTTGTAGTCGAGATTGTGGCGCTCTGG-3′
pSK PCP F53A FP	5′-GGCCAGGAGTGCACCTGTGCTCTACAACCTGCAGAA-3′
pSK PCP RP	5′-CAGCCACTTCATAAAGCAGCAAAACT-3′

digested with EcoRI. pGBK-PCP was digested with EcoRI and StuI, followed by gel extraction of the vector backbone containing the C-terminal domain (CTD) of PCP. Both fragments were ligated to generate the pGBK A57F PCP clone. pGBK PCP F53A was generated in two steps. The 176-bp PCP F53A-N-terminal domain (NTD) was PCR amplified using the pGBK-PCP template and PCP FP (EcoRI) and PCP F53A RP primers. PCR product and the pGBKT7 vector were digested with EcoRI and PstI, followed by ligation to generate the pGBK F53A PCP-NTD clone. The pGBK F53A PCP-NTD clone was digested with PstI, followed by dephosphorylation. pGBK-PCP was digested with PstI, followed by gel extraction of the 320-bp PCP CTD fragment. The 320-bp PCP CTD and pGBK-F53A PCP NTD were ligated to generate the pGBK F53A PCP. pGBK PCP E58A was generated as follows. PCP-NTD was PCR amplified using the pGBK-PCP template and PCP FP (EcoRI) and PCP E58A RP primers. The E58A PCP NTD PCR product was digested with EcoRI. pGBK-PCP was digested with EcoRI and StuI followed by gel extraction of the ~7.5-kb fragment. It was ligated with the E58A PCP NTD fragment to generate the pGBK-PCP E58A. The pGBK F53A E58A PCP double mutant was generated as follows. The PCP NTD was PCR amplified using the template pGBK-F53A PCP and PCP FP (EcoRI) and PCP E58A RP primers, followed by EcoRI digestion. pGBK-PCP was digested with EcoRI and StuI, followed by gel extraction of the ~7.5-kb fragment. Both fragments were ligated to generate the double mutant. pGBK C50A PCP and pGBK-C52A PCP clones were generated by site-directed mutagenesis using the pGBK-PCP template and PCP C50A FP and PCP C50A RP primers for pGBK C50A PCP and PCP C52A FP and PCP C52A RP primers for pGBK C52A PCP, respectively. DpnI treatment was given to the PCR mix to digest the parental methylated DNA template. pGEX-eIF2AK4 CTD was generated as follows. eIF2AK4 CTD was PCR amplified using the pDONOR223-eIF2AK4 template and hGCN2 CTD y2h FP (EcoRI) and GCN2 RP (XhoI) primers. The PCR product and pGEX-4T-1 vector were digested with EcoRI and XhoI, followed by ligation of both vector and insert. pET-eIF2AK4 CTD was generated as follows. pGEX-eIF2AK4 CTD was restriction digested with EcoRI and XhoI, followed by gel extraction of the eIF2AK4 CTD fragment. The pET-28a(+) vector was digested with EcoRI and XhoI, followed by ligation of the eIF2AK4 CTD fragment into the vector. pGAD-eIF2AK4 CTD was generated as follows. eIF2AK4 was PCR amplified using the pCDNA-eIF2AK4-His template and hGCN2 CTD FP (EcoRI) and GCN2 RP (XhoI) primers. The PCR product and pGADT7 vector were digested with EcoRI and XhoI, followed by ligation. pUNO-PCP F53A-Flag was generated as follows. The PCP F53A fragment was PCR amplified using the pGBKT7-PCP template and PCP FP (AgeI) and PCP-Flag RP (NheI) primers. The PCP F53A PCR product was digested with AgeI and NheI. The pUNO-hIPSI vector was digested with AgeI and NheI, followed by gel extraction of the ~3.2-kb fragment and ligation with the PCP F53A fragment. The pSKHEV2 PCP F53A construct was generated by site-directed mutagenesis using the pSKHEV2 template and pSK PCP F53A FP and pSK PCP RP primers. DpnI treatment was given to the PCR product to digest the parental methylated DNA template. All clones were verified by restriction digestion and confirmed by DNA sequencing.

Yeast transformation and yeast two-hybrid assay. The Y2H Gold strain was cotransformed with the desired plasmids by the lithium acetate method, following previously described protocol (11). The cotransformation mixture was plated on LT^- synthetic dropout (SD) media. After 3 days, cotransformed colonies were used for replica plating onto the following selection media plates: $LTHA^-$, LTH-A^{r+}, LT^- plus X-α-gal, LTH^- plus 5mM 3-AT, LTH^- plus 10 mM 3-AT, and LTH^- plus 20 mM 3-AT, and LTH^- plus 30 mM 3-AT. The growth of replica-plated colonies was monitored for 3 days at 30°C in a humidified incubator, followed by visual scoring of colony growth on a scale of "+" to "+++" where +, ++, and+++ indicate poor, moderate, and strong growth, respectively. Lack of growth was scored as "−".

Mammalian cell culture, transfection, Flag affinity purification, coimmunoprecipitation, and Western blotting. Huh7 (human hepatoma) cells were maintained in Dulbecco's modified Eagle medium (DMEM) containing 10% fetal bovine calf serum (FBS) and 50 IU/mL penicillin and streptomycin in 5% CO_2 as described earlier (11). Cells were seeded at 70% confluence and transfected with pUNO-PCP WT-Flag or pUNO-PCP F53A-

Flag using Lipofectamine 3000, following the manufacturer's protocol (Thermo Scientific, MA, USA). Six hours posttransfection, culture medium was replaced with DMEM plus 10% FBS. After 48 h of transfection, cells were washed with phosphate-buffered saline (PBS) (10 mM PO_4^{3-}, 137 mM NaCl, and 2.7 mM KCl) at ambient temperature, resuspended in lysis buffer (20 mM Tris-Cl, pH 7.5, 150 mM NaCl, 1% Triton X-100, 1 mM EDTA, 1 mM EGTA, 2.5 mM sodium pyrophosphate, 1 mM β-glycerol phosphate, and 1 mM Na_3VO_4) supplemented with protease inhibitor cocktail, and incubated on ice for 2 h. It was followed by centrifugation for 10 min at 13,000 $\times$ *g* and 4°C. The supernatant was incubated with Flag-agarose beads at 4°C for 2 h on a flip-flop rocker, followed by centrifugation for 1 min at 1,000 $\times$ *g* and 4°C. Beads were washed thrice with lysis buffer, and bound proteins were eluted by incubating the beads for 15 min at 4°C with Flag peptide (100 μg/mL in PBS). The protein concentration was determined by bicinchoninic acid assay (BCA), and single-use aliquots were stored at −80°C. Purified WT PCP and F53A mutant PCP proteins were confirmed by SDS-PAGE followed by Western blot analysis using anti-Flag antibody and silver staining. Coimmunoprecipitation and Western blotting were done as described (11). Briefly, cells were washed once with PBS and lysed in lysis buffer supplemented with protease inhibitor cocktail (Roche, Indianapolis, USA) as described above. An equal amount of protein lysate was incubated with 1 μg of corresponding antibody overnight at 4°C on a flip-flop rocker, followed by incubation with 100 μL of 20% protein A-Sepharose beads for 1 h. The beads were washed three times in lysis buffer and incubated at 95°C for 5 min in Laemmli buffer (62.5 mM Tris-Cl, pH 6.8, 2% SDS, 10% glycerol, 50 mM dithiothreitol [DTT], and 0.01% bromophenol blue). Samples were resolved by SDS-PAGE, followed by Western blot analysis using required primary antibodies and corresponding horseradish peroxidase-conjugated secondary antibodies. Protein signals were detected by enhanced chemiluminescence using a commercially available kit (Bio-Rad, CA, USA). Representative images of Western blots have been shown in the figures. Unless mentioned otherwise, data are representative of three independent experiments.

Protein expression and purification. eIF2AK4-CTD was cloned as an N-terminal GST fusion into bacterial expression vector pGEX4T-1 followed by transformation into BL21(DE3) pLysS cells. Cells were grown to A_{600} of ~0.5, followed by addition of 0.5 mM IPTG (isopropyl-β-D-thiogalactopyranoside) and incubation for 6 h at 25°C with 250 rpm shaking. Cells were centrifuged at 5,000 $\times$ *g* for 5 min at 4°C, and cell pellets were washed once in binding buffer and sonicated at 4°C (6 cycles of 10-s on, 30-s off pulse), followed by centrifugation for 10 min at 13,000 $\times$ *g*. Supernatants containing the soluble protein fraction were incubated with glutathione agarose beads for 2 h at 4°C on a flip-flop rocker, followed by three washes with binding buffer. GST-eIF2AK4-CTD protein was eluted by incubation with 20 mM glutathione in 50 mM Tris (pH 8.0) and 150 mM NaCl.

N-terminal His-eIF2AK4-CTD cloned in the pET28a(+) vector was transformed into BL21(DE3) pLysS cells. Cells were grown to A_{600} of ~0.5, followed by addition of 0.5 mM IPTG and incubation for 6 h at 37°C. The soluble protein fraction was obtained as described above and incubated with Ni-NTA superflow agarose (Thermo Scientific, MA, USA) for 2 h at 4°C, followed by three washes in binding buffer. Bound proteins were eluted in 500 mM imidazole.

Purified GST-eIF2AK4-CTD and His-eIF2AK4-CTD proteins were confirmed by SDS-PAGE followed by Coomassie blue staining and Western blotting using anti-GST (for GST-eIF2AK4-CTD) and anti-His (for His-eIF2AK4-CTD) antibodies. Concentrations of the eluted proteins were estimated by running them along with known quantities of purified bovine serum albumin (BSA) and quantifying approximate concentrations according to band intensities. Proteins were stored as single-use aliquots at −80°C.

Pulldown assays. Soluble protein fractions from *E. coli* expressing the GST-eIF2AK4-CTD and GST proteins (25 μg each) were mixed with protease inhibitor cocktail and glutathione agarose beads and incubated on a flip-flop rocker at 4°C for 2 h. Samples were centrifuged at 500 $\times$ *g* for 1 min at 4°C to settle the beads containing the bound proteins. Beads were washed thrice in wash buffer as described earlier. Beads were resuspended in binding buffer, and 2.5 μg purified His-eIF2AK4-CTD or His-ORF2 was added to it, followed by 1 h incubation at 4°C on a flip-flop rocker. Beads were washed 3 times, and bound proteins were eluted by incubation at 95°C for 5 min in Laemmli buffer. Aliquots of the eluted proteins were resolved by SDS-PAGE followed by Coomassie blue staining and Western blotting using anti-His and anti-GST antibodies. We loaded 10% of proteins used for the pulldown assay as input. Wherever required, purified WT PCP or F53A mutant PCP was added to the samples along with His-eIF2AK4-CTD.

***In vitro* phosphorylation assay.** Endogenous eIF2AK4 was immunoprecipitated from Huh7 hepatoma cells using anti-eIF2AK4 antibody. Cells were lysed in lysis buffer followed by incubation with 20 μg eIF2AK4 antibody for 16 h on a flip-flop rocker at 4°C. We added 40 μL and 200 μL protein G Dynabeads (50% [vol/vol]; Thermo Scientific, MA, USA) to mock and eIF2AK4 antibody-containing samples, respectively, followed by 1 h incubation under the same condition. Beads were washed thrice in IP buffer and two times in kinase buffer (25 mM Tris-Cl [pH 7.5], 5 mM β-glycerol phosphate, 2 mM DTT, 0.1 mM sodium orthovanadate, and 10 mM $MgCl_2$). Beads were resuspended in 270 μL kinase buffer and aliquoted into 9 tubes. Mock was resuspended in 60 μL kinase buffer. Thirty microliters each of mock and eIF2AK4 IP samples were Western blotted using anti-eIF2AK4 antibody to confirm the IP. Different combinations of protein and ATP were added to the remaining tubes. We used 1 μg recombinant human eIF2α protein and 4 μL of 10 mM ATP. We used 1 and 2 μg of Flag-affinity purified PCP and ORF2 proteins. The reaction mixture was incubated for 45 min at 30°C. The reaction was terminated by adding 20 μL of 3$\times$ Laemmli buffer (87.5 mM Tris [pH 6.8], 6% SDS, 30% glycerol, 150 mM DTT, and 0.03% bromophenol blue) and incubating at 95°C for 5 min. Aliquots of the samples were resolved by SDS-PAGE and S51-phosphorylated eIF2α, and total eIF2α was detected by Western blot analysis using antibodies against p-eIF2α (S51) and total eIF2α. PCP and ORF2 proteins were detected using anti-Flag antibody.

Immunofluorescence assay and qRT-PCR. Immunofluorescence assay (IFA) and qRT-PCR were done as described (6). Briefly, 6 μg *in vitro*-synthesized genomic RNA (g1-HEV and g1-HEV PCP F53A mut) was transfected into Huh7 cells at 70% confluence in 6-well tissue culture dishes using Lipofectamine 3000 in Opti-MEM. Six hours posttransfection, culture medium was replaced with DMEM plus 10% FBS. Seventy-two hours posttransfection, cells were seeded at 50% confluence into 6-well dishes containing coverslips and

allowed to grow for another 72 h. Next, cells were fixed for 30 min with 4% paraformaldehyde and washed thrice with PBS, followed by incubation with 100% methanol for 5 min at −20°C. Next, cells were washed three times with PBS and incubated with blocking solution (5% normal goat serum, 5% BSA in PBS, and 0.5% Tween 20) for 60 min at room temperature followed by washing with PBS. Primary antibodies (in PBS, 0.5% Tween 20, 5% BSA, and 1% normal goat serum) were added to coverslips and incubated overnight at 4°C. Primary antibody dilutions were anti-ORF2 (1:1,000) and anti-helicase (1:1,000). The next day, coverslips were washed three times with PBS and incubated for 1 h with 1:500 dilution of goat anti-rabbit Alexa Fluor 594 (in PBS, 0.5% Tween 20, 5% BSA). Coverslips were washed thrice in PBS and mounted on glass slides using antifade gold containing DAPI. Images were acquired using a 60× objective in a confocal microscope (Olympus FV3000) and analyzed by FluoView software. Helicase and ORF2-positive cells from 10 random fields were counted, and the percentages of positive cells were calculated. Data are represented as mean ± standard deviation (SD) of 3 experiments. *P* values were calculated by Student's *t* test (two-tailed). A *P* value of <0.05 was considered significant. For qRT-PCR, Huh7 hepatoma cells were transfected with 6 μg *in vitro*-synthesized genomic RNA (WT g1-HEV and F53A mutant PCP g1-HEV). Forty-eight hours posttransfection, total RNA was isolated using TRI reagent (MRC Inc., OH, USA). Reverse transcription was done using FireScript RT cDNA synthesis kit (Solis BioDyne, Tartu, Estonia), following the manufacturer's instructions. qRT-PCR was done using the 5× Hot FirePol EvaGreen qPCR Mix Plus (ROX), following the manufacturer's instructions. HEV RNA levels were normalized to that of GAPDH and presented as mean ± SD. *P* values were calculated by Student's *t* test. A *P* value of <0.05 was considered significant.

Luciferase assay. Cell-based assay was performed using HEK293T cells in white-walled 96-well plates as reported earlier (54). For induction of interferon response, a constitutively active mutant of RIG-I, R-C (only the CARD domains) was used. Briefly, a plasmid expressing R-C (10 ng per well) was cotransfected with plasmids expressing wild-type PCP or the F53A mutant PCP or vector alone (50 ng per well) as control, as well as two luciferases, the firefly luciferase driven by an IFN-β promoter and a *Renilla* luciferase driven by a thymidine kinase (TK) promoter. *Renilla* luciferase was used as an internal control. All transfections were performed using Lipofectamine 2000, following the manufacturer's protocol. Luciferase activity was measured 24 h posttransfection using Promega Dual-Glo luciferase assay kit, following the manufacturer's protocol using Synergy HT multimode microplate reader (Bio-Tek, USA). The ratios of firefly to *Renilla* luciferase values were converted to percentages, and the data were plotted as percentage of activity. Values obtained for R-C without PCP or its mutant were considered 100%, and the rest of the values were normalized to R-C values.

Statistics. Data are represented as mean ± standard deviation (SD) of three independent experiments. *P* values were calculated by two-tailed Student's *t* test (paired two samples for means). A minimum of 3 independent values were used for calculating SD and *t* test. The mean is shown for two values.

Data availability. This study does not include any data deposited in external repositories. All data and reagents generated in this study are available upon request.

ACKNOWLEDGMENTS

This study was funded by the Department of Biotechnology, Government of India, grant to M.S. and THSTI core grant to M.S. A.K. is supported by a senior research fellowship from the Indian Council of Medical Research, Government of India. C.T.R.-K. acknowledges the FRGS grant of GGSIPU.

REFERENCES

1. Nimgaonkar I, Ding Q, Schwartz RE, Ploss A. 2018. Hepatitis E virus: advances and challenges. Nat Rev Gastroenterol Hepatol 15:96–110. https://doi.org/10.1038/nrgastro.2017.150.
2. Kamar N, Lhomme S, Abravanel F, Marion O, Peron JM, Alric L, Izopet J. 2016. Treatment of HEV infection in patients with a solid-organ transplant and chronic hepatitis. Viruses 8:222. https://doi.org/10.3390/v8080222.
3. Kumar A, Beniwal M, Kar P, Sharma JB, Murthy NS. 2004. Hepatitis E in pregnancy. Int J Gynaecol Obstet 85:240–244. https://doi.org/10.1016/j.ijgo.2003.11.018.
4. Patra S, Kumar A, Trivedi SS, Puri M, Sarin SK. 2007. Maternal and fetal outcomes in pregnant women with acute hepatitis E virus infection. Ann Intern Med 147:28–33. https://doi.org/10.7326/0003-4819-147-1-200707030-00005.
5. Melgaço JG, Gardinali NR, Mello VDMD, Leal M, Lewis-Ximenez LL, Pinto MA. 2018. Hepatitis E: update on prevention and control. BioMed Res Int 2018:5769201. https://doi.org/10.1155/2018/5769201.
6. Nair VP, Anang S, Subramani C, Madhvi A, Bakshi K, Srivastava A, Nayak B, Ranjith Kumar CT, Surjit M Shalimar. 2016. Endoplasmic reticulum stress induced synthesis of a novel viral factor mediates efficient replication of genotype-1 hepatitis E virus. PLoS Pathog 12:e1005521. https://doi.org/10.1371/journal.ppat.1005521.
7. Sehgal D, Thomas S, Chakraborty M, Jameel S. 2006. Expression and processing of the hepatitis E virus ORF1 nonstructural polyprotein. Virol J 3:38. https://doi.org/10.1186/1743-422X-3-38.
8. Suppiah S, Zhou Y, Frey TK. 2011. Lack of processing of the expressed ORF1 gene product of hepatitis E virus. Virol J 8:245. https://doi.org/10.1186/1743-422X-8-245.
9. Perttilä J, Spuul P, Ahola T. 2013. Early secretory pathway localization and lack of processing for hepatitis E virus replication protein pORF1. J Gen Virol 94:807–816. https://doi.org/10.1099/vir.0.049577-0.
10. Parvez MK. 2013. Molecular characterization of hepatitis E virus ORF1 gene supports a papain-like cysteine protease (PCP)-domain activity. Virus Res 178:553–556. https://doi.org/10.1016/j.virusres.2013.07.020.
11. Subramani C, Nair VP, Anang S, Mandal SD, Pareek M, Kaushik N, Srivastava A, Saha S, Nayak B, Ranjith-Kumar CT, Surjit M Shalimar. 2018. Host-virus protein interaction network reveals the involvement of multiple host processes in the life cycle of hepatitis E virus. mSystems 3:e00135-17. https://doi.org/10.1128/mSystems.00135-17.
12. Metzger K, Bentaleb C, Hervouet K, Alexandre V, Montpellier C, Saliou JM, Ferrié M, Camuzet C, Rouillé Y, Lecoeur C, Dubuisson J, Cocquerel L, Aliouat-Denis CM. 2022. Processing and subcellular localization of the hepatitis E virus replicase: identification of candidate viral factories. Front Microbiol 13:828636. https://doi.org/10.3389/fmicb.2022.828636.
13. Fieulaine S, Tubiana T, Bressanelli S. 2023. De novo modelling of HEV replication polyprotein: five-domain breakdown and involvement of flexibility in functional regulation. Virology 578:128–140. https://doi.org/10.1016/j.virol.2022.12.002.
14. Szkolnicka D, Pollán A, Da Silva N, Oechslin N, Gouttenoire J, Moradpour D. 2019. Recombinant hepatitis E viruses harboring tags in the ORF1 protein. J Virol 93:e00459-19. https://doi.org/10.1128/JVI.00459-19.
15. Magden J, Takeda N, Li T, Auvinen P, Ahola T, Miyamura T, Merits A, Kääriäinen L. 2001. Virus-specific mRNA capping enzyme encoded by hepatitis E virus. J Virol 75:6249–6255. https://doi.org/10.1128/JVI.75.14.6249-6255.2001.
16. Anang S, Subramani C, Nair VP, Kaul S, Kaushik N, Sharma C, Tiwari A, Ranjith-Kumar CT, Surjit M. 2016. Identification of critical residues in hepatitis E virus macro domain involved in its interaction with viral methyltransferase and ORF3 proteins. Sci Rep 6:25133. https://doi.org/10.1038/srep25133.

17. Parvez MK. 2017. Mutational analysis of hepatitis E virus ORF1 "Y domain": effects on RNA replication and virion infectivity. World J Gastroenterol 23:590–602. https://doi.org/10.3748/wjg.v23.i4.590.
18. Shafat Z, Hamza A, Deeba F, Parvez MK, Parveen S. 2021. Molecular insights into the Y domain of hepatitis E virus using computational analyses. Beni-Suef Univ J Basic Appl Sci 10:1–14. https://doi.org/10.1186/s43088-021-00154-3.
19. Koonin EV, Gorbalenya AE, Purdy MA, Rozanov MN, Reyes GR, Bradley DW. 1992. Computer-assisted assignment of functional domains in the nonstructural polyprotein of hepatitis E virus: delineation of an additional group of positive-strand RNA plant and animal viruses. Proc Natl Acad Sci U S A 89:8259–8263. https://doi.org/10.1073/pnas.89.17.8259.
20. Li C, Debing Y, Jankevicius G, Neyts J, Ahel I, Coutard B, Canard B. 2016. Viral macro domains reverse protein ADP-ribosylation. J Virol 90:8478–8486. https://doi.org/10.1128/JVI.00705-16.
21. Nan Y, Yu Y, Ma Z, Khattar SK, Fredericksen B, Zhang YJ. 2014. Hepatitis E virus inhibits type I interferon induction by ORF1 products. J Virol 88:11924–11932. https://doi.org/10.1128/JVI.01935-14.
22. Karpe YA, Lole KS. 2011. Deubiquitination activity associated with hepatitis E virus putative papain-like cysteine protease. J Gen Virol 92:2088–2092. https://doi.org/10.1099/vir.0.033738-0.
23. Shukla P, Nguyen HT, Torian U, Engle RE, Faulk K, Dalton HR, Bendall RP, Keane FE, Purcell RH, Emerson SU. 2011. Cross-species infections of cultured cells by hepatitis E virus and discovery of an infectious virus–host recombinant. Proc Natl Acad Sci U S A 108:2438–2443. https://doi.org/10.1073/pnas.1018878108.
24. Shukla P, Nguyen HT, Faulk K, Mather K, Torian U, Engle RE, Emerson SU. 2012. Adaptation of a genotype 3 hepatitis E virus to efficient growth in cell culture depends on an inserted human gene segment acquired by recombination. J Virol 86:5697–5707. https://doi.org/10.1128/JVI.00146-12.
25. Pudupakam RS, Huang YW, Opriessnig T, Halbur PG, Pierson FW, Meng XJ. 2009. Deletions of the hypervariable region (HVR) in open reading frame 1 of hepatitis E virus do not abolish virus infectivity: evidence for attenuation of HVR deletion mutants in vivo. J Virol 83:384–395. https://doi.org/10.1128/JVI.01854-08.
26. Pudupakam RS, Kenney SP, Córdoba L, Huang YW, Dryman BA, LeRoith T, Pierson FW, Meng XJ. 2011. Mutational analysis of the hypervariable region of hepatitis E virus reveals its involvement in the efficiency of viral RNA replication. J Virol 85:10031–10040. https://doi.org/10.1128/JVI.00763-11.
27. Kadaré G, Haenni AL. 1997. Virus-encoded RNA helicases. J Virol 71:2583–2590. https://doi.org/10.1128/JVI.71.4.2583-2590.1997.
28. Karpe YA, Lole KS. 2010. NTPase and 5′ to 3′ RNA duplex-unwinding activities of the hepatitis E virus helicase domain. J Virol 84:3595–3602. https://doi.org/10.1128/JVI.02130-09.
29. Karpe YA, Lole KS. 2010. RNA 5′-triphosphatase activity of the hepatitis E virus helicase domain. J Virol 84:9637–9641. https://doi.org/10.1128/JVI.00492-10.
30. Graff J, Torian U, Nguyen H, Emerson SU. 2006. A bicistronic subgenomic mRNA encodes both the ORF2 and ORF3 proteins of hepatitis E virus. J Virol 80:5919–5926. https://doi.org/10.1128/JVI.00046-06.
31. Surjit M, Jameel S, Lal SK. 2007. Cytoplasmic localization of the ORF2 protein of hepatitis E virus is dependent on its ability to undergo retrotranslocation from the endoplasmic reticulum. J Virol 81:3339–3345. https://doi.org/10.1128/JVI.02039-06.
32. Surjit M, Varshney B, Lal SK. 2012. The ORF2 glycoprotein of hepatitis E virus inhibits cellular NF-κB activity by blocking ubiquitination mediated proteasomal degradation of IκBα in human hepatoma cells. BMC Biochem 13:7. https://doi.org/10.1186/1471-2091-13-7.
33. Hingane S, Joshi N, Surjit M, Ranjith-Kumar CT. 2020. Hepatitis E virus ORF2 inhibits RIG-I mediated interferon response. Front Microbiol 11:656. https://doi.org/10.3389/fmicb.2020.00656.
34. Ding Q, Heller B, Capuccino JM, Song B, Nimgaonkar I, Hrebikova G, Contreras JE, Ploss A. 2017. Hepatitis E virus ORF3 is a functional ion channel required for release of infectious particles. Proc Natl Acad Sci U S A 114:1147–1152. https://doi.org/10.1073/pnas.1614955114.
35. Surjit M, Oberoi R, Kumar R, Lal SK. 2006. Enhanced α1 microglobulin secretion from hepatitis E virus ORF3-expressing human hepatoma cells is mediated by the tumor susceptibility gene 101. J Biol Chem 281:8135–8142. https://doi.org/10.1074/jbc.M509568200.
36. Nagashima S, Takahashi M, Jirintai S, Tanaka T, Nishizawa T, Yasuda J, Okamoto H. 2011. Tumour susceptibility gene 101 and the vacuolar protein sorting pathway are required for the release of hepatitis E virions. J Gen Virol 92:2838–2848. https://doi.org/10.1099/vir.0.035378-0.
37. He M, Wang M, Huang Y, Peng W, Zheng Z, Xia N, Xu J, Tian D. 2016. The ORF3 protein of genotype 1 hepatitis E virus suppresses TLR3-induced NF-κB signaling via TRADD and RIP1. Sci Rep 6:27597. https://doi.org/10.1038/srep27597.
38. Costa-Mattioli M, Walter P. 2020. The integrated stress response: from mechanism to disease. Science 368p:eaat5314. https://doi.org/10.1126/science.aat5314.
39. Bergmann M, Garcia-Sastre A, Carnero E, Pehamberger H, Wolff K, Palese P, Muster T. 2000. Influenza virus NS1 protein counteracts PKR-mediated inhibition of replication. J Virol 74:6203–6206. https://doi.org/10.1128/jvi.74.13.6203-6206.2000.
40. Mulvey M, Arias C, Mohr I. 2007. Maintenance of endoplasmic reticulum (ER) homeostasis in herpes simplex virus type 1-infected cells through the association of a viral glycoprotein with PERK, a cellular ER stress sensor. J Virol 81:3377–3390. https://doi.org/10.1128/JVI.02191-06.
41. del Pino J, Jiménez JL, Ventoso I, Castelló A, Muñoz-Fernández MÁ, de Haro C, Berlanga JJ. 2012. GCN2 has inhibitory effect on human immunodeficiency virus-1 protein synthesis and is cleaved upon viral infection. PLoS One 7:e47272. https://doi.org/10.1371/journal.pone.0047272.
42. Qiu H, Garcia-Barrio MT, Hinnebusch AG. 1998. Dimerization by translation initiation factor 2 kinase GCN2 is mediated by interactions in the C-terminal ribosome-binding region and the protein kinase domain. Mol Cell Biol 18:2697–2711. https://doi.org/10.1128/MCB.18.5.2697.
43. Lageix S, Zhang J, Rothenburg S, Hinnebusch AG. 2015. Interaction between the tRNA-binding and C-terminal domains of yeast Gcn2 regulates kinase activity in vivo. PLoS Genet 11:e1004991. https://doi.org/10.1371/journal.pgen.1004991.
44. Berlanga JJ, Ventoso I, Harding HP, Deng J, Ron D, Sonenberg N, Carrasco L, de Haro C. 2006. Antiviral effect of the mammalian translation initiation factor 2α kinase GCN2 against RNA viruses. EMBO J 25:1730–1740. https://doi.org/10.1038/sj.emboj.7601073.
45. Kubota H, Obata T, Ota K, Sasaki T, Ito T. 2003. Rapamycin-induced translational derepression of GCN4 mRNA involves a novel mechanism for activation of the eIF2α kinase GCN2. J Biol Chem 278:20457–20460. https://doi.org/10.1074/jbc.C300133200.
46. Gupta J, Kaul S, Srivastava A, Kaushik N, Ghosh S, Sharma C, Batra G, Banerjee M, Nayak B, Ranjith-Kumar CT, Surjit M Shalimar. 2020. Expression, purification and characterization of the Hepatitis E virus like-particles in the Pichia pastoris. Front Microbiol 11:141. https://doi.org/10.3389/fmicb.2020.00141.
47. Kaushik N, Subramani C, Anang S, Muthumohan R, Nayak B, Ranjith-Kumar CT, Surjit M Shalimar. 2017. Zinc salts block hepatitis E virus replication by inhibiting the activity of viral RNA-dependent RNA polymerase. J Virol 91:e00754-17. https://doi.org/10.1128/JVI.00754-17.
48. Mudhasani R, Tran JP, Retterer C, Kota KP, Whitehouse CA, Bavari S. 2016. Protein kinase R degradation is essential for Rift Valley fever virus infection and is regulated by SKP1-CUL1-F-box (SCF) FBXW11-NSs E3 ligase. PLoS Pathog 12:e1005437. https://doi.org/10.1371/journal.ppat.1005437.
49. Hakki M, Marshall EE, De Niro KL, Geballe AP. 2006. Binding and nuclear relocalization of protein kinase R by human cytomegalovirus TRS1. J Virol 80:11817–11826. https://doi.org/10.1128/JVI.00957-06.
50. Vincent HA, Ziehr B, Moorman NJ. 2017. Mechanism of protein kinase R inhibition by human cytomegalovirus pTRS1. J Virol 91:e01574-16. https://doi.org/10.1128/JVI.01574-16.
51. Qian W, Zhu S, Sobolev AY, Wek RC. 1996. Expression of vaccinia virus K3L protein in yeast inhibits eukaryotic initiation factor-2 kinase GCN2 and the general amino acid control pathway. J Biol Chem 271:13202–13207. https://doi.org/10.1074/jbc.271.22.13202.
52. Castilho BA, Shanmugam R, Silva RC, Ramesh R, Himme BM, Sattlegger E. 2014. Keeping the eIF2 alpha kinase Gcn2 in check. Biochim Biophys Acta 1843:1948–1968. https://doi.org/10.1016/j.bbamcr.2014.04.006.
53. Emerson SU, Nguyen H, Graff J, Stephany DA, Brockington A, Purcell RH. 2004. In vitro replication of hepatitis E virus (HEV) genomes and of an HEV replicon expressing green fluorescent protein. J Virol 78:4838–4846. https://doi.org/10.1128/jvi.78.9.4838-4846.2004.
54. Madhvi A, Hingane S, Srivastav R, Joshi N, Subramani C, Muthumohan R, Khasa R, Varshney S, Kalia M, Vrati S, Surjit M, Ranjith-Kumar CT. 2017. A screen for novel hepatitis C virus RdRp inhibitor identifies a broad-spectrum antiviral compound. Sci Rep 7:5816. https://doi.org/10.1038/s41598-017-04449-3.